Environmental Science & Technology

Article

pubs.acs.org/est

Highly Sensitive Strategy for Hg^{2+} Detection in Environmental Water Samples Using Long Lifetime Fluorescence Quantum Dots and Gold Nanoparticles

Dawei Huang, Chenggang Niu,* Min Ruan, Xiaoyu Wang, Guangming Zeng,* and Canhui Deng

College of Environmental Science and Engineering, Key Laboratory of Environmental Biology and Pollution Control, Ministry of Education, Hunan University, Changsha 410082, People's Republic of China

Supporting Information

ABSTRACT: The authors herein described a time-gated fluorescence resonance energy transfer (TGFRET) sensing strategy employing water-soluble long lifetime fluorescence quantum dots and gold nanoparticles to detect trace Hg^{2+} ions in aqueous solution. The water-soluble long lifetime fluorescence quantum dots and gold nanoparticles were functionalized by two complementary ssDNA, except for four deliberately designed T−T mismatches. The quantum dot acted as the energy-transfer donor, and the gold nanoparticle acted as the energy-transfer acceptor. When Hg^{2+} ions were present in the aqueous solution, DNA hybridization will occur because of the formation of T−Hg^{2+}−T complexes. As a result, the quantum dots and gold nanoparticles are brought into close proximity, which made the energy transfer occur from quantum dots to gold nanoparticles, leading to the fluorescence intensity of quantum dots to decrease obviously. The decrement fluorescence intensity is proportional to the concentration of Hg^{2+} ions. Under the optimum conditions, the sensing system exhibits the same liner range from 1×10^{-9} to 1×10^{-8} M for Hg^{2+} ions, with the detection limits of 0.49 nM in buffer and 0.87 nM in tap water samples. This sensor was also used to detect Hg^{2+} ions from samples of tap water, river water, and lake water spiked with Hg^{2+} ions, and the results showed good agreement with the found values determined by an atomic fluorescence spectrometer. In comparison to some reported colorimetric and fluorescent sensors, the proposed method displays the advantage of higher sensitivity. The TGFRET sensor also exhibits excellent selectivity and can provide promising potential for Hg^{2+} ion detection.

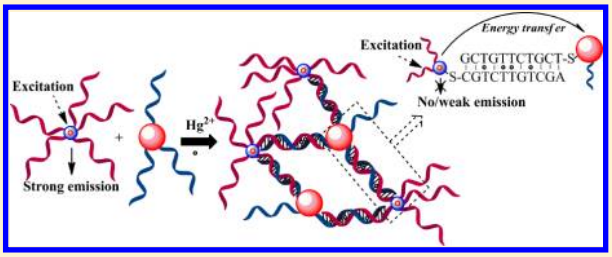

1. INTRODUCTION

As one of the most toxic heavy metals, Hg^{2+} is a widespread and severe environmental pollutant and has serious adverse effects on human health and the environment.[1,2] Solvated Hg^{2+}, one of the most stable inorganic forms of mercury, is a caustic and carcinogenic material with high cellular toxicity.[3,4] To date, the contamination of drinking water by water-soluble Hg^{2+} is still the most common.[5] Therefore, it is important to monitor Hg^{2+} levels with sensitivity and selectivity in aqueous systems. The development of novel Hg^{2+} detection methods that are rapid, low-cost, sensitive, and applicable to aqueous systems has become an urgent need to protect our environment and health.

Traditional methods for Hg^{2+} detection in aqueous systems, including atomic absorption/emission spectroscopy, cold vapor atomic absorption spectrometry (CV-AAS), and ultraviolet−visible (UV−vis) spectrophotometry, usually have disadvantages of labor-intensive, time-consuming, and large sample volume requirements.[6−9] To overcome these weaknesses, researchers made great efforts to develop various methods for the analysis of Hg^{2+}, including fluorescent and colorimetric sensors.[10−18] Fluorescence resonance energy transfer (FRET) methods between a fluorescent donor and an acceptor, in particular, are extremely attractive and arouse the interest of researchers.[19−25] In conventional FRET sensors, organic molecules were often used as the energy donor and acceptor. Recently, many studies focus on the inorganic quantum dots (QDs) because of their tunable narrow-band emission and broad excitation spectra. QDs can substitute for organic dyes as the alternative and excellent energy donors. Many FRET sensors based on QDs and dyes with high sensitivity and reliability have been presented.[26−31] Gold nanoparticles (GNPs) have been of great interest because of their high extinction coefficient and a broad absorption spectrum in visible light that is overlapped with the emission wavelength of usual energy donors. Researchers have devoted a lot of effort to fabricate sensors based on GNPs as the acceptor for DNA, small molecules, or protein detection.[22,32−38] More recently, a detecting trace Hg^{2+} method, which used QDs as the donor and GNPs as the acceptor, was developed.[25] In these FRET sensors, which use organic dyes or QDs as the donor, the background signals might interfere with the fluorescence of organic dyes or QDs, affecting the sensitivity of the sensors. Therefore, it should be desirable to develop a novel method, which uses long

Received: July 21, 2012
Revised: October 20, 2012
Accepted: March 21, 2013
Published: March 21, 2013

lifetime fluorophore as the donor or acceptor, to decrease the background noises on the basis of time-gated fluorescence assay. The authors found that Mn-doping QDs are good choices that have high quantum yield and long lifetime fluorescence.[39−43]

It is well-known that oligonucletides can interact with metal ions with high specificity. It has been previously demonstrated that Hg^{2+} can selectively bind in between two DNA thymine (T) bases and promote these T−T mismatches to form stable T−Hg^{2+}−T base pairs.[44,45] The Hg^{2+}-mediated T−Hg^{2+}−T pairs are more stable and have higher melting temperature than the Watson−Crick A−T pairs. Hg^{2+} can be incorporated into the DNA duplex without largely altering the double helical structure because the van der Waals radius of mercury (≈1.44 Å) is smaller than the base pair spacing of the DNA duplex (≈3.4 Å).[44] Considering all of these mentioned above, a time-gated fluorescence resonance energy transfer (TGFRET) sensor combined the advantages of GNPs and Mn-doping QDs and used the specificity and stable structure of T−Hg^{2+}−T for Hg^{2+} detection in aqueous solution. The proposed method exhibits higher sensitivity than some sensors previously reported and also has high selectivity toward Hg^{2+} even in the presence of other competitive heavy metal ions. Furthermore, Hg^{2+} ion detections in tap water, river water, and lake water samples are performed to demonstrate the practical use of this sensor. The developed sensor with high sensitivity and selectivity may be an alternative method for Hg^{2+} ion detection in environmental, biomedical, and other applications.

2. EXPERIMENTAL SECTION

2.1. Chemicals and Apparatus. All oligonucleotides used in the present study were synthesized and high-performance liquid chromatography (HPLC)-purified by Shanghai Sangon Biological Engineering Technology and Services Co., Ltd. (Shanghai, China) and dissolved in ultrapure water (18.3 MΩ cm) produced by a Millpore water purification system. Their base sequences are as follows: **1**, 5′-SH-CGTCTTGTCGA-3′; **2**, 5′-SH-TCGTCTTGTCG-3′. $AuCl_3$·HCl·$4H_2O$ was purchased from Shanghai Institute of Fine Chemical Materials (Shanghai, China). Sulfur powder (99.999%), 1-octadecence (ODE, tech. 90%), oleylamine (OAm, tech. 70%), and 1-octadecylamine (ODA, 97%) were purchased from Aldrich. Manganese acetate tetrahydrate (99%) and all of the solvents were purchased from Fisher Scientific Company. Nitric acid (≥69.5%, TraceSELECT) was purchased from Fluka. Cadmium acetate hydrate (99.999%) and zinc stearate (count as ZnO ≈ 14%) were purchased from Alfa Aesar. Quinine sulfate (99+%) was purchased from Acros. Oleic acid and 3-mercaptopropionic acid (MPA, 99+%) were purchased from Sigma-Aldrich. The chemicals were used as received without further purification. Cadmium myristate was self-made according to the literature method.[39] All other chemicals used were of analytical grade and were used without further purification. Ultrapure water was used throughout the experiments.

UV−vis absorption spectra were recorded using a Shimadzu UV spectrophotometer (UV-2550, Kyoto, Japan). The time-gated fluorescence intensities were measured and recorded with a Perkin-Elmer LS-55 spectrofluorimeter (U.K.). The transmission electron microscopy (TEM) image of QDs was measured with a JEOL JEM-3010 transmission electron microscope (Beijing, China). Atomic fluorescence measurements were performed on an atomic fluorescence spectrometer (AFS-9700, Beijing, China).

Phosphate-buffered saline (PBS) buffer (100 mM) was prepared by mixing an appropriate content of 200 mM Na_2HPO_4 and 200 mM NaH_2PO_4. The composition of hybridization buffer, stock buffer, and washing buffer was 10 mM PBS buffer (pH 7.4) and 100 mM $NaNO_3$. Otherwise, 2 M NaCl was also prepared.

2.2. Synthesis of Mn-Doping CdS/ZnS Core/Shell QDs. Mn-doped CdS/ZnS core/shell QDs were prepared according to a three-step synthesis method.[39,40] Briefly, in the first step, CdS/ZnS core/shell QDs were synthesized with a CdS core diameter of 3.1 nm and a ZnS shell by the typical core/shell growth method. In the second step (dopant growth), a hexane solution of resulting core/shell particles was added to a mixture solution of ODE and OAm (ODE/OAm = 3:1), and then hexane was removed under vacuum. Under an argon flow, the CdS/ZnS core/shell QD solution was heated to 280 °C, and then a $Mn(OAc)_2$ solution and sulfur solution [$Mn(OAc)_2$ and sulfur at a molar ratio of 1:1] were introduced into the hot solution by dropwise addition. The doping level was controlled by adding a different amount of $Mn(OAc)_2$ and sulfur solutions. The synthesis was stopped after 20 min of reaction. In the third step, the resulting CdS/ZnS core/shell QDs with Mn dopants at the surface were further overcoated with ZnS shell through alternate injections of the solutions of zinc stearate in ODE and sulfur in ODE. The growth time was 10 min after each injection. Importantly, when the desired shell thickness was achieved, a large excess of zinc stearate in ODE solution was injected into the reaction system. After 25 min, oleic acid was introduced into the solution and the synthesis was stopped by cooling the reaction solution to room temperature. The resulting QDs were isolated by adding acetone and further purified by 3 precipitation−redispersion cycles using methanol and toluene. Final particles were dispersed in hexane.

The lack of water solubility of the prepared QDs hindered their reaction with the water-soluble alkylthiol-capped oligonucleotides. Therefore, the authors used ligand exchange with 3-mercaptopropionic acid to prepare the water-soluble QDs according to the literature.[46]

2.3. Synthesis of GNPs. All glassware and a mechanical stirrer used for the synthesis were thoroughly cleaned in aqua regia (3 parts HCl and 1 part HNO_3), rinsed with ultrapure water, and then oven-dried prior to use. The colloidal solution of GNPs was synthesized by means of citrate reduction of $AuCl_3$·HCl·$4H_2O$.[47] A total of 5 mL of 38.8 mM sodium citrate was rapidly added to a boiled 50 mL of 1 mM $HAuCl_4$ solution with vigorous stirring in a 250 mL round-bottom flask equipped with a condenser. The color changed from light yellow to wine red. Boiling was continued for 10 min; the heating mantle was then removed; and stirring was continued for an additional 15 min. After the solution was cooled to room temperature, the prepared GNP solution was stored in the 4 °C refrigerator before use. The size of the nanoparticles was typically ∼13 nm in average diameter. The concentration of the GNPs was ∼17 nM, which was determined according to Beer's law using UV−vis spectroscopy based on the extinction coefficient of 2.7×10^8 M^{-1} cm^{-1} at λ = 520 nm for 13 nm particles.[48]

2.4. Preparation of DNA-Functionalized GNPs. According to the literature with slight modifications,[49] 20 mL of 17 nM GNPs was incubated with 20 μL of 0.1 mM oligonucleotides overnight. After standing for 16 h at 50 °C, the mixed solution was changed into 0.1 M NaCl and 10 mM phosphate buffer (pH 7.4) by the addition of the necessary salts

and was kept at 50 °C for 40 h. To remove unreacted oligonucleotides, the oligonucleotide-conjugated GNPs were purified 3 times by centrifugation at 13 200 rpm for 30 min. The final product was redispersed into 5 mL of PBS buffer (10 mM, pH 7.4) to make a stock solution and stored at 4 °C for future usage. The number of oligonucleotide probes immobilized on the GNPs was estimated by measuring the absorbance difference at 260 nm before and after modification with oligonucleotides. The average oligonucleotide loadings were about three oligonucleotides per GNP, and the final concentration of GNPs was 52 nM.

2.5. Preparation of DNA-Functionalized Mn-Doping CdS/ZnS Core/Shell QDs. DNA-functionalized QDs were prepared according to a previously published protocol with minor modifications.[46] The QD solution and oligonucleotide solution were mixed together at a ratio of 12 oligonucleotides per QD (4 mL of 164 nM QDs mixed with 80 μL of 0.1 mM oligonucleotides). After standing for 12 h, the mixed solution was brought to 0.15 M NaCl, and the particles were aged for an additional 12 h. The NaCl concentration was then raised to 0.3 M, and the mixture was allowed to stand for a further 40 h before centrifugalization using centrifugal filter devices (Amicon Ultra-0.5). Finally, the QDs were redispersed into 5 mL of PBS buffer (10 mM, pH 7.4) by vortex and stored at 4 °C for future usage. The number of oligonucleotide probes immobilized on the GNPs was also estimated by measuring the absorbance difference at 260 nm before and after modification with oligonucleotides. The average oligonucleotide loadings were about five oligonucleotides per QD, and the final concentration of QDs was 112 nM.

2.6. Procedures for Hg^{2+} Detection. First, 30 μL of 112 nM DNA/QDs, 120 μL of 52 nM DNA/GNPs, and 50 μL of 0.01 M PBS buffer were mixed uniformly by vortex. Then, different concentrations of Hg^{2+} (50 μL) were added to the mixture solution. Finally, the time-gated fluorescence emission intensities of different concentrations of Hg^{2+} were monitored after the completion of the hybrid reaction. For the sensitivity experiment, the concentrations of Hg^{2+} were of 0, 0.5, 1.0, 2.0, 4.0, 6.0, 8.0, 10.0, 20.0, 40.0, 60.0, 80.0, 100.0, 200.0, 500.0, 1000.0, and 5000.0 nM, respectively. For the optimizing experiment of hybridization time, 200 nM was selected as the Hg^{2+} concentration to determine the optimum hybridization time. Various metal ion salts of 200 nM were used in the selectivity experiment. The metal ion salts are as follows: $Mn(Ac)_2$, $Ba(NO_3)_2$, $Ni(Ac)_2$, $CuSO_4$, $CaCl_2$, $Cr(NO_3)_2$, $Co(NO_3)_2$, $Cd(NO_3)_2$, $MgSO_4$, $Zn(Ac)_2$, $Al_2(SO_4)_3$, $Fe_2(SO_4)_3$, and $Pb(NO_3)_2$. The river water and lake water samples were taken from Xiang River and Taozi Lake. The time-gated fluorescence signal was measured and recorded by a Perkin-Elmer LS-55 spectrofluorimeter. The parameters of the spectrofluorimeter are set as follows: λ_{ex}, 400 nm; λ_{em}, 609 nm; delay time, 0.1 ms; gate time, 1.0 ms; and excitation slit and emission slit, 15 nm.

3. RESULTS AND DISCUSSION

3.1. Experimental Principle and Sensing Scheme. In the present study based on the specificity and stable structure of T−Hg^{2+}−T, the authors fabricated a TGFRET sensor for highly sensitive and selective detection of Hg^{2+}. The authors designed two 11 base complementary ssDNA strands (**1** and **2**), except for four deliberately designed T−T mismatches. Oligonucleotides **1** and **2** are both 5′-terminal-modified with −SH and contain two parts: the four thymine mercury-binding sequence and the linker sequence of seven bases. The two oligonucleotides could not form a self-folded structure by Hg^{2+}. Oligonucleotide **1** was connected with ∼5 nm-sized Mn doping of CdS/ZnS core/shell QDs (probe A), and oligonucleotide **2** was connected with the ∼13 nm diameter GNPs (probe B). Figure 1A schematically showed the fundamental Hg^{2+} assay.

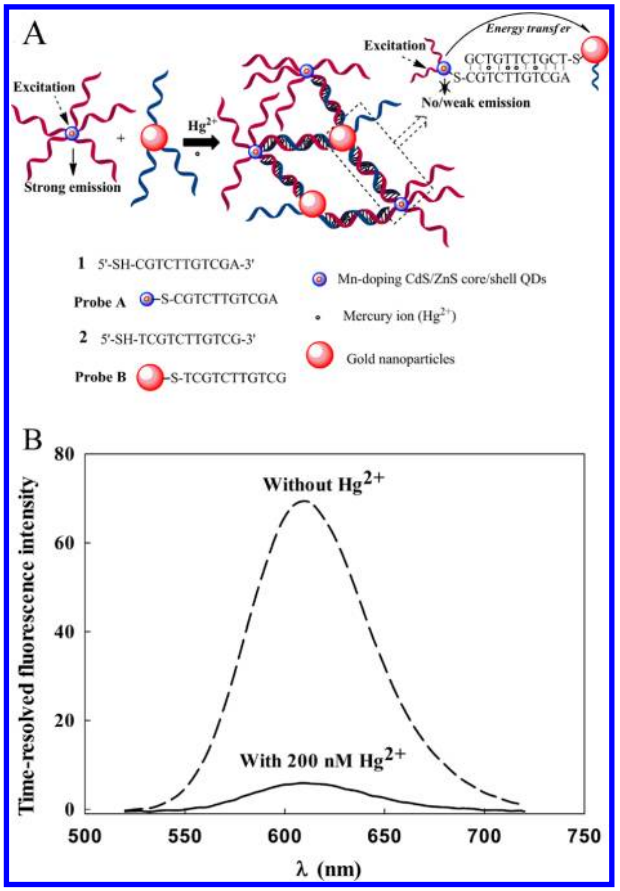

Figure 1. (A) Schematic description of TGFRET sensing of Hg^{2+} based on the Hg^{2+}-mediated formation in DNA duplexes. When Hg^{2+} was introduced to the aqueous solution, DNA hybridization will occur because of the formation of T−Hg^{2+}−T complexes. As a result, the QDs and GNPs were brought into close proximity, which made the energy transfer occur from QDs to GNPs, leading to the fluorescence intensity decrease. The drawing of QD- and GNP-modified ssDNA is only a graphic presentation. (B) Time-gated fluorescence emission intensities without and with the addition of 200 nM Hg^{2+}.

The QD acted as the energy donor; the GNP acted as the energy acceptor; and the hybridized double-stranded DNA acts as the linker between the QD and the GNP. The QDs with ∼5 nm in diameter showed the fluorescence emission at 609 nm under light excitation (see Figures S1 and S2 of the Supporting Information). The fluorescence emission band of the QDs exhibited partial spectral overlap with the absorbance band of the ∼13 nm-sized GNPs (see Figure S3 of the Supporting Information). In the absence of Hg^{2+} ions, the probes A and B are not capable of hybridization and are well-dispersed in the aqueous solution because of the four mismatched T−T base pairs, which made the left seven base pairs not stable enough. In this case, the time-gated fluorescence of QDs was observed at 609 nm, with light excitation at 400 nm. When Hg^{2+} ions were present in the aqueous solution, the hybridization between the two probes will occur because of the formation

of T−Hg^{2+}−T complexes. The QDs and GNPs were brought into close proximity, which made the energy transfer occur from QDs to GNPs, leading to the fluorescence intensity of QDs to decrease sharply (panels A and B of Figure 1). Otherwise, a control experiment was used to investigate if Hg^{2+} ions have an effect on the fluorescence of QDs, in which Hg^{2+} ions were added to a solution only containing probe A. The results indicated that Hg^{2+} ions make negligible contribution toward quenching the fluorescence of QDs in the present work (see Figure S4 of the Supporting Information).

Fluorescence quenching contains static and dynamic quenching. In the case of dynamic quenching, fluorescence quenching occurs without any permanent change in the molecules. However, the excited-state lifetime of fluorophore will be shortened. In static quenching, a complex is formed between the fluorophore and the quencher. In general, this complex is nonfluorescent, and the absorption spectra will be changed. The experiments showed that the absorption spectra of QDs have no obvious change before and after the addition of GNPs to the QD solution in the proposed method. The excited-state lifetime of QDs is reduced in the presence of GNPs. Consequently, the quenching is not static quenching, and the QDs and GNPs cannot form a ground-state complex in the proposed study.

3.2. Optimization of the Hybridization Conditions. In the present strategy, the hybridization time, hybridization temperature, and media pH played crucial roles for the detection sensitivity. Generally, a longer hybridization time yields a more stable fluorescence signal. The fluorescence signal was recorded along with the hybridization time increasing (Figure 2). It is found that the fluorescence signal decreased with the hybridization time increasing, then reached a minimum at 18 min, and kept almost a constant value until 30 min. To ensure the completeness of hybridization between probes A and B, the authors choose 20 min as the optimum hybridization time. Furthermore, if the hybridization temperature is too low, a longer hybridization time is required; if the hybridization temperature is higher than the melting temperature, the DNA duplex will denature. Taking into account operational convenience, room temperature (20−22 °C) was selected as the operational temperature for all experiments. To benefit the hybridization reaction, the media pH for all of the experimental steps was maintained at 7.4.

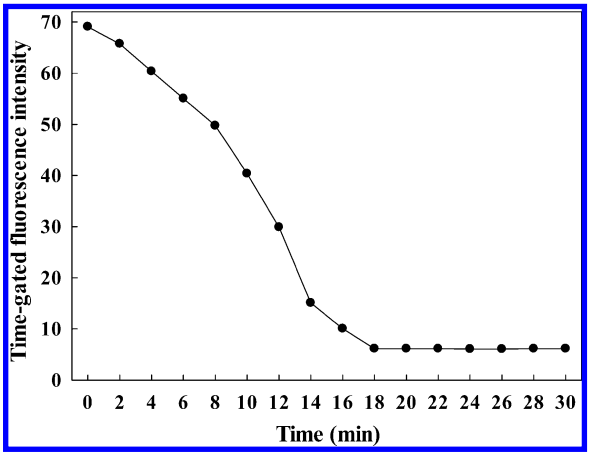

Figure 2. Optimizing experiment of the hybridization time. A value of 200 nM was selected as the Hg^{2+} concentration to determine the optimum hybridization time.

3.3. Sensitivity for Hg^{2+}. According to the above standard procedures and under the optimized assay conditions, different concentrations of Hg^{2+} were added to the buffer and the time-gated fluorescence emission intensity was measured to evaluate the sensitivity of the TGFRET sensor. The various concentrations of Hg^{2+} were 0, 0.5, 1.0, 2.0, 4.0, 6.0, 8.0, 10.0, 20.0, 40.0, 60.0, 80.0, 100.0, 200.0, 500.0, 1000.0, and 5000.0 nM. The experimental results were shown in Figure 3A. With the increase of the Hg^{2+} concentration, the time-gated fluorescence emission intensities decreased gradually. Even at very low concentrations of Hg^{2+}, the time-gated fluorescence emission intensity exhibited perceptible change, which indicated that Hg^{2+} could be detected with high sensitivity in this proposed TGFRET sensor. The authors discussed the fluorescence quenching efficiency using the equation $I = (F_0 - F)/F_0$, where F_0 and F were the fluorescence intensities without and with different concentrations of Hg^{2+}, respectively (see Figure S5 of the Supporting Information). Figure S5 of the Supporting Information showed that the fluorescence quenching rate of

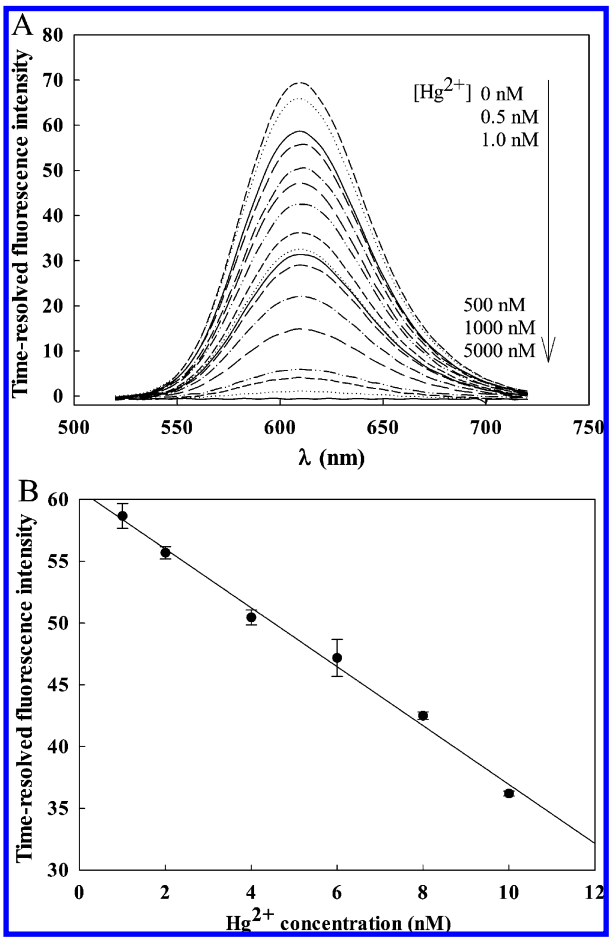

Figure 3. (A) Time-gated fluorescence emission spectra of the working solutions containing the ssDNA−QDs and ssDNA−GNPs after the addition of various concentrations (0−5000 nM) of Hg^{2+} in pure hybridization buffer. (B) Linear relationship between the time-gated fluorescence intensity and Hg^{2+} concentration in buffer. The concentrations of Hg^{2+} were 1.0, 2.0, 4.0, 6.0, 8.0, and 10 nM. Every data point was the mean of three measurements. The error bars are the standard deviation.

dx.doi.org/10.1021/es302967n | Environ. Sci. Technol. 2013, 47, 4392−4398

nearly 100% was observed when the Hg^{2+} ion concentration was up to 5000 nM.

3.4. Calibration Curves of Hg^{2+} Detection. The decrement time-gated fluorescence emission intensity was found to be linear with the concentration of Hg^{2+} in the range from 1×10^{-9} to 1×10^{-8} M (Figure 3B). The equation for the resulting calibration plot was $y = -2.3844x + 60.77$ (x was the concentration of Hg^{2+}, and y was the time-gated fluorescence intensity), with a correlation coefficient of 0.9964. According to the standard deviation of 0.39 for the blank signal with 20 parallel measurements, a limit of detection of approximately 0.49 nM (0.1 ppb) was estimated by 3 times the standard deviation rule. The limit of detection was sufficient to monitor Hg^{2+} changes from basal levels, which was lower than the standards of the World Health Organization (WHO) and United States Environmental Protection Agency (U.S. EPA). The WHO and U.S. EPA regulate the maximum allowable levels of Hg^{2+} in drinking water to be 6 and 2 ppb, respectively. The limit of detection of the proposed TGFRET sensor for Hg^{2+} detection was much improved in comparison to those previously reported colorimetric sensors, fluorescent sensors, and FRET sensors,[12−14,17,18,24,25,50−53] although all of these sensors had a similar molecular recognition mechanism (T−Hg^{2+}−T) (see Table S1 of the Supporting Information). Generally speaking, because of the limitations of the colorimetric sensor itself, the sensitivity of the colorimetric sensor is lower than that of the fluorescent sensor. In comparison to common fluorescent methods, the time-gated fluorescent method could reduce the background noises caused by autofluorescence from biological samples and the luminescence from optical components, which will limit the sensitivity of the fluorescent methods. Hence, the sensitivity of the time-gated fluorescent method with long lifetime fluorescence QDs is higher than some fluorescent methods that use fluorophore with short lifetime fluorescence. The calibration equation can serve as the quantitative basis for the determination of trace Hg^{2+} content in the sample.

3.5. Selectivity for Hg^{2+}. To evaluate the selectivity of this protocol, two control experiments were conducted. First, the difference of fluorescence intensities for Hg^{2+} and other metal ions, including Mn^{2+}, Ba^{2+}, Ni^{2+}, Cu^{2+}, Ca^{2+}, Cr^{2+}, Co^{2+}, Cd^{2+}, Mg^{2+}, Zn^{2+}, Al^{3+}, Fe^{3+}, and Pb^{2+} detection, under optimum conditions was compared. As indicated in Figure 4, in contrast to significant response as observed for Hg^{2+}, negligible signal response was observed upon the addition of other tested metal ions. Hence, the results showed excellent selectivity toward Hg^{2+} over other metal ions because of the specificity structure of T−Hg^{2+}−T. Second, Hg^{2+} and other metal ions were mixed to form a mixture solution as a sample for the anti-jamming capability testing of the TGFRET sensor (Figure 4). The fluorescence quenching efficiency was obviously higher than other samples without Hg^{2+}. These results clearly indicated that the approach is not only insensitive to other metal ions but also selective toward Hg^{2+} in their presence. As noted above, the present sensor had excellent anti-jamming capability and outstanding selectivity.

3.6. Assay of Hg^{2+} Concentrations in Tap Water Samples. The application of the proposed method was evaluated for the determination of Hg^{2+} in tap water. All of the tap water samples were spiked with Hg^{2+} at different concentration levels. The different concentrations of Hg^{2+} were 0, 0.5, 1.0, 2.0, 4.0, 6.0, 8.0, 10.0, 20.0, 40.0, 60.0, 80.0, 100.0, 200.0, 500.0, 1000.0, and 5000.0 nM. The results were shown in Figure S6A of the Supporting Information; the time-gated fluorescence intensity decreased with the increasing concentration of Hg^{2+}. The fluorescence quenching efficiency was also very excellent according to Figure S7 of the Supporting Information. Figure S6B of the Supporting Information showed the calibration curves of Hg^{2+} detection in tap water samples. The equation for the resulting calibration plot was $y = -2.0644x + 58.28$ (x was the concentration of Hg^{2+}, and y was the time-gated fluorescence intensity), with a correlation coefficient of 0.9776. According to the standard deviation of 0.60 for the blank signal with 20 parallel measurements, a limit of detection of approximately 0.87 nM (0.18 ppb) was estimated by 3 times the standard deviation rule, which increased a few compared to that of the buffer assay. These results showed that the strategy is also workable in tap water samples.

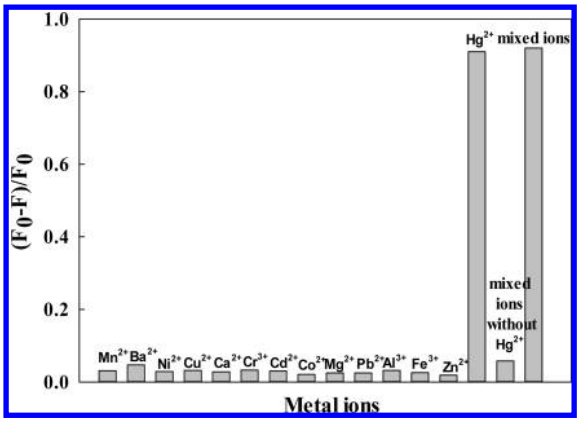

Figure 4. Fluorescence quenching efficiency in the presence of various metal ions. The concentration of each metal ion is 200 nM. The fluorescence intensities were 68.58 (buffer), 66.45 (Mn^{2+}), 65.36 (Ba^{2+}), 66.59 (Ni^{2+}), 66.39 (Cu^{2+}), 66.66 (Ca^{2+}), 66.32 (Cr^{2+}), 66.52 (Cd^{2+}), 67.14 (Co^{2+}), 66.87 (Mg^{2+}), 66.87 (Pb^{2+}), 66.39 (Al^{3+}), 66.80 (Fe^{3+}), 67.28 (Zn^{2+}), 6.17 (Hg^{2+}), 64.60 (mixed ions without Hg^{2+}), and 5.49 (mixed ions).

3.7. Environmental Water Sample Analysis Using the Proposed Method and Atomic Fluorescence Spectroscopy (AFS). To test the practical application of the proposed method, several environmental water samples spiked with Hg^{2+}, with concentrations of 0, 2.0, 4.0, and 10.0 nM, were tested using the proposed method and AFS. The environmental water samples used in the study were tap water, river water, and lake water samples. The river water and lake water samples were filtered by qualitative filter paper and then centrifuged for 20 min at 12 000 rpm. The concentrations of total mercury in river water and lake water samples were measured to be less than 0.1 nM by AFS. The samples spiked with different concentrations of Hg^{2+} were detected according to the general procedure with four replicates. The results were summarized in Table 1 and showed good agreement with the found values determined by AFS. The results revealed that the present sensor can also work in environmental samples. Although the authors have demonstrated here the detection of Hg^{2+} ions only, this sensing strategy can in principle be used to detect different analytes, such as other metal ions or proteins, by substituting the T−Hg^{2+}−T complexes with other specificity structures that selectively bind the other analytes. It is believed that this sensing strategy may be an alternative method for the analysis of Hg^{2+} in environmental samples.

dx.doi.org/10.1021/es302967n | Environ. Sci. Technol. 2013, 47, 4392−4398

Table 1. Determination of Hg^{2+} in Environment Water Samples Using the Proposed Method and AFS

	Hg^{2+} (nM)		
sample	added	proposed method (mean[a] ± SD[b])	AFS (mean ± SD)
tap water 1	0	c	<0.1
tap water 2	2.0	1.98 ± 0.10	2.04 ± 0.04
tap water 3	4.0	4.08 ± 0.13	4.04 ± 0.07
tap water 4	10.0	10.03 ± 0.58	10.03 ± 0.01
river water 1	0	c	<0.1
river water 2	2.0	2.03 ± 0.12	2.03 ± 0.04
river water 3	4.0	4.03 ± 0.15	4.05 ± 0.03
river water 4	10.0	9.97 ± 0.45	10.1 ± 0.19
lake water 1	0	c	<0.1
lake water 2	2.0	2.03 ± 0.11	2.05 ± 0.03
lake water 3	4.0	4.05 ± 0.13	4.06 ± 0.04
lake water 4	10.0	10.0 ± 0.15	10.2 ± 0.22

[a]Mean of four determinations. [b]SD = standard deviation. [c]No Hg^{2+} concentration could be detected.

■ ASSOCIATED CONTENT

Ⓢ Supporting Information

TEM image of Mn-doping CdS/ZnS core/shell QDs (Figure S1), UV−vis absorption and time-gated fluorescence emission spectra of water-soluble Mn-doping CdS/ZnS core/shell QDs (Figure S2), absorption of 13 nm GNPs and time-gated fluorescence emission spectra of ssDNA-functionalized QDs (Figure S3), fluorescence emission spectra of QD-modified ssDNA in the absence and presence of 10, 100, and 1000 nM Hg^{2+} (Figure S4), calibration curve of fluorescence quenching efficiency as a function of the Hg^{2+} concentration in buffer samples (Figure S5), time-gated fluorescence emission spectra of working solutions containing the ssDNA−QDs and ssDNA−GNPs after the addition of various concentrations (0−5000 nM) of Hg^{2+} in tap water samples and linear relationship between the time-gated fluorescence intensity and Hg^{2+} concentration in tap water samples (Figure S6), calibration curve of fluorescence quenching efficiency as a function of the Hg^{2+} concentration in tap water samples (Figure S7), and comparison of sensitivity for Hg^{2+} assay methods (Table S1). This material is available free of charge via the Internet at http://pubs.acs.org.

■ AUTHOR INFORMATION

Corresponding Author

*Telephone: +86-731-88823820. Fax: +86-731-88822829. E-mail: cgniu@hnu.edu.cn and/or cgniu@hotmail.com (C.N.); zgming@hnu.edu.cn (G.Z.).

Notes

The authors declare no competing financial interest.

■ ACKNOWLEDGMENTS

This work was financially supported by the National Natural Science Foundation of China (20977026 and 51039001), the National 863 High Technology Research Foundation of China (2006AA06Z407), the Research Fund for the Doctoral Program of Higher Education of China (20090161110009), the project-sponsored by SRF for ROCS, SEM (521294018), and the Fundamental Research for the Central University of Hunan University (531107040375). Special thanks are given to Y. Charles Cao and his group at the University of Florida for kind assistance in the synthesis of Mn-doping CdS/ZnS core/shell QDs.

■ REFERENCES

(1) Hylander, L. D.; Goodsite, M. E. Environmental costs of mercury pollution. *Sci. Total Environ.* **2006**, *368*, 352−370.

(2) Nolan, E. M.; Lippard, S. J. Tools and tactics for the optical detection of mercuric ion. *Chem. Rev.* **2008**, *108*, 3443−3480.

(3) Wojcik, D. P.; Godfrey, M. E.; Christie, D.; Haley, B. E. Mercury toxicity presenting as chronic fatigue, memory impairment and depression: Diagnosis, treatment, susceptibility, and outcomes in a New Zealand general practice setting. *Neuroendocrinol. Lett.* **2006**, *27*, 415−423.

(4) Sekowski, J. W.; Malkas, L. H.; Wei, Y.; Hickey, R. J. Mercuric ion inhibits the activity and fidelity of the human cell DNA synthesome. *Toxicol. Appl. Pharmacol.* **1997**, *145*, 268−276.

(5) Jarup, L. Hazards of heavy metal contamination. *Br. Med. Bull.* **2003**, *68*, 167−182.

(6) Bernaus, A.; Gaona, X.; Esbrí, J. M.; Higueras, P.; Falkenberg, G.; Valiente, M. Microprobe techniques for speciation analysis and geochemical characterization of mine environments: The mercury district of Almaden in Spain. *Environ. Sci. Technol.* **2006**, *40*, 4090−4095.

(7) Butler, O. T.; Cook, J. M.; Harrington, C. F.; Hill, S. J.; Rieuwerts, J.; Miles, D. L. Atomic spectrometry update. Environmental analysis. *J. Anal. At. Spectrom.* **2006**, *21*, 217−243.

(8) Li, Y.; Chen, C.; Li, B.; Sun, J.; Wang, J.; Gao, Y.; Zhao, Y.; Chai, Z. Elimination efficiency of different reagents for the memory effect of mercury using ICP−MS. *J. Anal. At. Spectrom.* **2006**, *21*, 94−96.

(9) Leermakers, M.; Baeyens, W.; Quevauviller, P.; Horvat, M. Mercury in environmental samples: speciation, artifacts and validation. *Trends Anal. Chem.* **2005**, *24*, 383−393.

(10) Nolan, E. M.; Lippard, S. J. Turn-on and ratiometric mercury sensing in water with a red-emitting probe. *J. Am. Chem. Soc.* **2007**, *129*, 5910−5918.

(11) Wegner, S. V.; Okesli, A.; Chen, P.; He, C. Design of an emission ratiometric biosensor from MerR family proteins: A sensitive and selective sensor for Hg^{2+}. *J. Am. Chem. Soc.* **2007**, *129*, 3474−3475.

(12) Li, H. L.; Zhai, J. F.; Tian, J. Q.; Luo, Y. L.; Sun, X. P. Carbon nanoparticle for highly sensitive and selective fluorescent detection of mercury(II) ion in aqueous solution. *Biosens. Bioelectron.* **2011**, *26*, 4656−4660.

(13) Wang, Y.; Yang, F.; Yang, X. R. Colorimetric biosensing of mercury(II) ion using unmodified gold nanoparticle probes and thrombin-binding aptamer. *Biosens. Bioelectron.* **2010**, *25*, 1994−1998.

(14) Xu, X. W.; Wang, J.; Jiao, K.; Yang, X. R. Colorimetric detection of mercury ion (Hg^{2+}) based on DNA oligonucleotides and unmodified gold nanoparticles sensing system with a tunable detection range. *Biosens. Bioelectron.* **2009**, *24*, 3153−3158.

(15) Xue, X. J.; Wang, F.; Liu, X. G. One-step, room temperature, colorimetric detection of mercury (Hg^{2+}) using DNA/nanoparticle conjugates. *J. Am. Chem. Soc.* **2008**, *130*, 3244−3245.

(16) Zhang, L. B.; Li, T.; Li, B. L.; Li, J.; Wang, E. K. Carbon nanotube−DNA hybrid fluorescent sensor for sensitive and selective detection of mercury(II) ion. *Chem. Commun.* **2010**, *46*, 1476−1478.

(17) Lee, J. S.; Han, M. S.; Mirkin, C. A. Colorimetric detection of mercuric ion (Hg^{2+}) in aqueous media using DNA-functionalized gold nanoparticles. *Angew. Chem.* **2007**, *119*, 4171−4174.

(18) Li, D.; Wieckowska, A.; Willner, I. Optical analysis of Hg^{2+} ions by oligonucleotide−gold nanoparticle hybrids and DNA-based machines. *Angew. Chem., Int. Ed.* **2008**, *47*, 3927−3931.

(19) Zhang, X.; Xiao, Y.; Qian, X. A ratiometric fluorescent probe based on FRET for imaging Hg^{2+} ions in living cells. *Angew. Chem., Int. Ed.* **2008**, *47*, 8025−8029.

(20) Chen, G. Z.; Jin, Y.; Wang, L.; Deng, J.; Zhang, C. X. Gold nanorods-based FRET assay for ultrasensitive detection of Hg^{2+}. *Chem. Commun.* **2011**, *47*, 12500−12502.

(21) Liu, B. Y.; Zeng, F.; Wu, G. F.; Wu, S. Z. A FRET-based ratiometric sensor for mercury ions in water with multi-layered silica nanoparticles as the scaffold. *Chem. Commun.* **2011**, *47*, 8913−8915.
(22) Liu, H.; Liang, G.; Abdel-Halim, E. S.; Zhu, J. J. A sensitive and selective quantum dots-based FRET biosensor for the detection of cancer marker type IV collagenase. *Anal. Methods* **2011**, *3*, 1797−1801.
(23) Kong, L. T.; Wang, J.; Zheng, G. C.; Liu, J. H. A highly sensitive protocol (FRET/SIMNSEF) for the determination of mercury ions: A unity of fluorescence quenching of graphene and enhancement of nanogold. *Chem. Commun.* **2011**, *47*, 10389−10391.
(24) Liu, C. W.; Huang, C. C.; Chang, H. T. Highly selective DNA-based sensor for lead(II) and mercury(II) ions. *Anal. Chem.* **2009**, *81*, 2383−2387.
(25) Li, M.; Wang, Q. Y.; Shi, X. D.; Hornak, L. A.; Wu, N. Q. Detection of mercury(II) by quantum dot/DNA/gold nanoparticle ensemble based nanosensor via nanometal surface energy transfer. *Anal. Chem.* **2011**, *83*, 7061−7065.
(26) Peng, H.; Zhang, L. J.; KjaÈllman, T. H. M.; Soeller, C.; Travas-Sejdic, J. DNA hybridization detection with blue luminescent quantum dots and dye-labeled single-stranded DNA. *J. Am. Chem. Soc.* **2007**, *129*, 3048−3049.
(27) Goldman, E. R.; Medintz, I. L.; Whitley, J. L.; Hayhurst, A.; Clapp, A. R.; Uyeda, H. T.; Deschamps, J. R.; Lassman, M. E.; Mattoussi, H. A hybrid quantum dot−antibody fragment fluorescence resonance energy transfer-based TNT sensor. *J. Am. Chem. Soc.* **2005**, *127*, 6744−6751.
(28) Tavares, A. J.; Noor, M. O.; Vannoy, C. H.; Algar, W. R.; Krull, U. J. On-chip transduction of nucleic acid hybridization using spatial profiles of immobilized quantum dots and fluorescence resonance energy transfer. *Anal. Chem.* **2012**, *84*, 312−319.
(29) Blaudeck, T.; Zenkevich, E. I.; Abdel-Mottaleb, M.; Szwaykowska, K.; Kowerko, D.; Cichos, F.; von Borczyskowski, C. Formation principles and ligand dynamics of nanoassemblies of CdSe quantum dots and functionalised dye molecules. *ChemPhysChem* **2012**, *13*, 959−972.
(30) Hardzei, M.; Artemyev, M.; Molinari, M.; Troyon, M.; Sukhanova, A.; Nabiev, I. Comparative efficiency of energy transfer from CdSe−ZnS quantum dots or nanorods to organic dye molecules. *ChemPhysChem* **2012**, *13*, 330−335.
(31) Chi, C. W.; Lao, Y. H.; Li, Y. S.; Chen, L. C. A quantum dot−aptamer beacon using a DNA intercalating dye as the FRET reporter: Application to label-free thrombin detection. *Biosens. Bioelectron.* **2011**, *26*, 3346−3352.
(32) Wang, H.; Wang, Y. X.; Jin, J. Y.; Yang, R. H. Gold nanoparticle-based colorimetric and "turn-on" fluorescent probe for mercury(II) ions in aqueous solution. *Anal. Chem.* **2008**, *80*, 9021−9028.
(33) Gueroui, Z.; Libchaber, A. Single-molecule measurements of gold-quenched quantum dots. *Phys. Rev. Lett.* **2004**, *98*, 166108-1−166108-4.
(34) Dyadyusha, L.; Yin, H.; Jaiswal, S.; Brown, T.; Baumberg, J. J.; Booy, F. P.; Melvin, T. Quenching of CdSe quantum dot emission, a new approach for biosensing. *Chem. Commun.* **2005**, 3201−3203.
(35) Huang, C. C.; Chiu, S. H.; Huang, Y. F.; Chang, H. T. Aptamer-functionalized gold nanoparticles for turn-on light switch detection of platelet-derived growth factor. *Anal. Chem.* **2007**, *79*, 4798−4804.
(36) Mandal, G.; Bardhan, M.; Ganguly, T. Occurrence of Förster resonance energy transfer between quantum dots and gold nanoparticles in the presence of a biomolecule. *J. Phys. Chem. C* **2011**, *115*, 20840−20848.
(37) Li, M.; Cushing, S. K.; Wang, Q. Y.; Shi, X. D.; Hornak, L. A.; Hong, Z. L.; Wu, N. Q. Size-dependent energy transfer between CdSe/ZnS quantum dots and gold nanoparticles. *J. Phys. Chem. Lett.* **2011**, *2*, 2125−2129.
(38) Zeng, Q.; Zhang, Y.; Liu, X.; Tu, L.; Kong, X.; Zhang, H. Multiple homogeneous immunoassays based on a quantum dots−gold nanorods FRET nanoplatform. *Chem. Commun.* **2012**, *48*, 1781−1783.
(39) Yang, Y.; Chen, O.; Angerhofer, A.; Cao, Y. C. Radial-position-controlled doping in CdS/ZnS core/shell nanocrystals. *J. Am. Chem. Soc.* **2006**, *128*, 12428−12429.
(40) Yang, Y.; Chen, O.; Angerhofer, A.; Cao, Y. C. On doping CdS/ZnS core/shell nanocrystals with Mn. *J. Am. Chem. Soc.* **2008**, *130*, 15649−15661.
(41) Norris, D. J. High-quality manganese-doped ZnSe nanocrystals. *Nano Lett.* **2001**, *1*, 3−7.
(42) Norris, D. J.; Efros, A. L.; Erwin, S. C. Doped nanocrystals. *Science* **2008**, *319*, 1776−1779.
(43) Nag, A.; Chakraborty, S.; Sarma, D. D. To dope Mn^{2+} in a semiconducting nanocrystal. *J. Am. Chem. Soc.* **2008**, *130*, 10605−10611.
(44) Miyake, Y.; Togashi, H.; Tashiro, M.; Yamaguchi, H.; Oda, S.; Kudo, M.; Tanaka, Y.; Kondo, Y.; Sawa, R.; Fujimoto, T.; Achinami, T.; Ono, A. Mercury^{II}-mediated formation of thymine−Hg^{II}−thymine base pairs in DNA duplexes. *J. Am. Chem. Soc.* **2006**, *128*, 2172−2173.
(45) Tanaka, Y.; Oda, S.; Yamaguchi, H.; Kondo, Y.; Kojima, C.; Ono, A. ^{15}N−^{15}N J-coupling across Hg^{II}: Direct observation of Hg^{II}-mediated T−T base pairs in a DNA duplex. *J. Am. Chem. Soc.* **2007**, *129*, 244−245.
(46) Mitchell, G. P.; Mirkin, C. A.; Letsinger, R. L. Programmed assembly of DNA functionalized quantum dots. *J. Am. Chem. Soc.* **1999**, *121*, 8122−8123.
(47) Katherine, C. G.; Freeman, R. G.; Michael, B. H.; Michael, J. N. Preparation and characterization monolayers. *Anal. Chem.* **1995**, *67*, 735−743.
(48) Haiss, W.; Thanh, N. T. K.; Aveyard, J.; Fernig, D. G. Determination of size and concentration of gold nanoparticles from UV−vis spectra. *Anal. Chem.* **2007**, *79*, 4215−4221.
(49) Storhoff, J. J.; Elghanian, R.; Mucic, R. C.; Mirkin, C. A.; Letsinger, R. L. One-pot colorimetric differentiation of polynucleotides with single base imperfections using gold nanoparticle probes. *J. Am. Chem. Soc.* **1998**, *120*, 1959−1964.
(50) Freeman, R.; Finder, T.; Willner, I. Multiplexed analysis of Hg^{2+} and Ag^{+} ions by nucleic acid functionalized CdSe/ZnS quantum dots and their use for logic gate operations. *Angew. Chem., Int. Ed.* **2009**, *48*, 7818−7821.
(51) Kanayama, N.; Takarada, T.; Maeda, M. Rapid naked-eye detection of mercury ions based on non-crosslinking aggregation of double-stranded DNA-carrying gold nanoparticles. *Chem. Commun.* **2011**, *47*, 2077−2079.
(52) Ono, A.; Togashi, H. Highly selective oligonucleotide-based sensor for mercury(II) in aqueous solutions. *Angew. Chem., Int. Ed.* **2004**, *43*, 4300−4302.
(53) Liu, X. F.; Tang, Y. L.; Wang, L. H.; Zhang, J.; Song, S. P.; Fan, C. H.; Wang, S. Optical detection of mercury(II) in aqueous solutions by using conjugated polymers and label-free oligonucleotides. *Adv. Mater.* **2007**, *19*, 1471−1474.